A&A 385, 909–920 (2002)
DOI: 10.1051/0004-6361:20020180

Astronomy & Astrophysics

Statistical study of $C^{18}O$ dense cloud cores and star formation

K. Tachihara[1], T. Onishi[2], A. Mizuno[2], and Y. Fukui[2]

[1] Max-Planck-Institut für extraterrestrische Physik, Giessenbachstraße, 85748 Garching, Germany
[2] Department of Astrophysics, Nagoya University, Chikusa-ku, Nagoya 464-8602, Japan

Received 31 May 2001 / Accepted 22 January 2002

Abstract. Dense molecular cloud cores are studied statistically in nearby ($d \leq 200$ pc) star-forming regions (SFRs) that show various modes of star formation. As a result of the $C^{18}O$ survey of NANTEN and the 4 m radio telescopes of Nagoya University, 179 cores have been collected in the SFRs of Taurus, the ρ Oph cloud, the Ophiuchus north region, the Lupus clouds, L1333, the Corona Australis cloud, Southern Coalsack, and the Pipe nebula, and their physical properties investigated. According to their star-formation activities, the cores are divided into 3 categories as 136 starless, 36 star-forming, and 7 cluster-forming cores. It is found that cores with active star formation tend to have larger $N(H_2)$, $n(H_2)$, and M. The mass function of the cores does not appear to follow a single power-law function, but the power-law index is subject to change with the mass range. The average star-formation efficiency (SFE) of the cores is roughly ∼10%, and the expected stellar mass function from the SFE approximates the stellar initial-mass function (IMF). Virial analysis shows that the star-forming cores are gravitationally more bound, with smaller virial ratios than the starless cores, while cluster-forming cores are marginally bound with moderate virial ratios. We found that turbulent decay is indicated by diminishing ΔV from the starless to the star-forming cores. It is suggested that the turbulent decay is necessary for star formation, while formed star clusters provide the turbulence and make the cores unbound. Molecular clouds associated with the clusters tend to have head-tail structures and the cluster formation takes place at the head. This implies that the clouds are affected by external shocks, which have triggered cluster formation. We suggest that star and cluster formation are strongly controlled by the initial amount of internal turbulence and the interaction with the external shocks.

Key words. ISM: clouds – ISM: kinematics and dynamics – ISM: molecules – radio lines: ISM – stars: formation

1. Introduction

Young stars are formed as a result of the gravitational collapse of dense molecular cloud cores. The dense cores typically have spherical shapes while lower density clouds are more elongated or filamentary. This implies that self gravity dominates the dense cores. They are frequently associated with embedded young stellar objects (YSOs) near the densest parts. Thus, dense cores are regarded as the birthplaces of stars and their properties are supposed to determine the characteristics of the young stars directly and/or indirectly.

Studies of many star-forming regions (SFRs) have revealed that the star-formation activity is not uniform, and we see various modes of it even in the vicinity of the sun in our galaxy. For example, star formation is very active and many massive stars are being formed in the Orion and Carina clouds, while in Taurus, star formation is moderate and isolated far from any massive stars (e.g., Kenyon & Hartman 1995). Active cluster formation is taking place in the ρ Oph (e.g., Wilking et al. 1989), Corona Australis (Harju et al. 1993; Neuhäuser et al. 2000), and the Cha I clouds (Cambrésy et al. 1998; Mizuno et al. 1999), but star formation is inactive in the Cha III cloud (Mizuno et al. 1999), the Oph North region (Nozawa et al. 1991; Tachihara et al. 2000), Lupus 5 (Tachihara et al. 1996), the Southern Coalsack cloud (Kato et al. 1999), and L1333 (Obayashi et al. 1998). With respect to the galaxy evolution, it is very important to know which mode of star formation is dominant, and what causes these variations. Even for molecular clouds in the same SFR such as Lupus and Chamaeleon, large difference in the star-forming activities can be seen. These variations of the mode of star formation may come from the difference in the circumstances in the regions, and the effects must appear in the physical properties of the molecular cloud cores. The best observational approach to this problem is statistical study of the dense cores collected from various SFRs.

Many attempts to investigate dense cores have been reported. A series of studies have been made of the dense cores in NH_3 toward optically opaque portions on the POSS plates and succeeded in detecting dense cores whose typical density and radius are $\sim 10^{4-5}$ cm^{-3} and 0.06 pc, respectively (e.g., Myers & Benson 1983;

Send offprint requests to: K. Tachihara,
e-mail: tatihara@mpe.mpg.de

Myers et al. 1991). A large number of NH_3 cores have been observed and many of them have associated YSOs. The work showed a direct link between the cores and the YSOs observationally. Myers & Fuller (1992) also reported that the non-thermal gas motion in the cores is important for the core dynamics. It is, however, somewhat biased towards the regions with higher background stellar densities due to the finding method, which prevents us from investigating the core properties statistically.

The NANTEN and the 4 m radio telescopes of Nagoya university have surveyed our galaxy for molecular clouds and cloud cores in $J = 1$–0 emission lines of CO isotopes of ^{12}CO, ^{13}CO, and $C^{18}O$ that trace different density regimes in the clouds of $n(H_2) \sim 10^2, 10^3$, and 10^4 cm^{-3}, respectively. The $C^{18}O$ dense cores have been surveyed without bias by picking up the denser parts of the molecular clouds from the preceding ^{13}CO mappings of all the clouds. This unbiased survey for the dense cores in $C^{18}O$ is an ideal method for finding embedded cores in a short observing time, because the extents of the dense cores are generally small on the sky and the $C^{18}O$ emission lines are weak. The unbiased core surveys have been done with the NANTEN telescope in 9 nearby SFRs of Taurus (Onishi et al. 1996), the ρ Oph cloud, the Oph North region (Tachihara et al. 2000), the Chamaeleon clouds (Mizuno et al. 1999), the Lupus clouds (Hara et al. 1999), L1333 (Obayashi et al. 1998), the Corona Australis cloud (the CrA cloud; Yonekura et al. 1999), the Pipe nebula (Onishi et al. 1999), and the Southern Coalsack cloud (Kato et al. 1999). Onishi et al. (1996, 1998) detected 40 cores from the Taurus cloud complex, and about half of them are associated with YSOs. They found that cores with larger column density, $N(H_2)$, tend to have YSOs. Obayashi et al. (1998) showed inactive star formation in L1333 and only one star-forming core with a relatively small virial mass (M_{Vir}) compared to the core mass (M). Tachihara et al. (2000) investigated the Ophiuchus region and found that the cores with smaller virial ratios (M_{Vir}/M) are more evolved towards star formation. We also suggested that the turbulent decay is necessary for star-formation and some quantified estimate of the energy release through the core contraction was calculated. Hara et al. (1999) compared the physical parameters of the cores in Lupus with those in other SFRs that show different star-formation activities. They found a common trend among the SFRs that the star-formation activity relates to $N(H_2)$ and the virial ratio. Mizuno et al. (1999) pointed out the significant difference in star forming efficiency (SFE) among the 3 Chamaeleon clouds, and suggested that the relative mass of the dense cores to the entire cloud mass relates to the star-formation activities.

These samples consist of star-forming cores with various activities. They contain no massive star-forming region like the Orion and Carina clouds, which are relatively distant. In this paper, we again investigate the comprehensive properties of the dense cores and the star-formation activities combining all the samples taken in many different SFRs in order to have a better understanding, using the most complete $C^{18}O$ core samples, of what the general property of the cores is that controls star formation.

Table 1. Star forming regions where the $C^{18}O$ cores are sampled.

star forming regions	distance (pc)	number of the cores	reference
Taurus	140	40	1, 2
L1333	180	13	3
Oph North	160	25	4
ρ Oph	160	15	4
Chamaeleon	140, 180	23	5
Lupus	150	36	6
CrA	130	8	7
Pipe nebula	160	14	8
Southern Coalsack	180	5	9

1. Onishi et al. (1996); 2. Onishi et al. (1998); 3. Obayashi et al. (1998); 4. Tachihara et al. (2000); 5. Mizuno et al. (1999); 6. Hara et al. (1999); 7. Yonekura et al. (1999); 8. Onishi et al. (1999); 9. Kato et al. (1999).

2. Samples of the cores

We have collected 174 $C^{18}O$ dense cores observed with the NANTEN and the 4 m radio telescopes of Nagoya university in nearby SFRs ($d \leq 200$ pc) from the studies done so far in the 9 regions (Table 1). This is the most extensive and largest dense-core survey ever done in $C^{18}O$. Most of the formed objects are low-mass stars, and only several Herbig Ae/Be stars exist in the ρ Oph, Lupus 3, the CrA, and the Cha I clouds. Thus, this work is limited to mainly low-mass star formation.

The NANTEN and the 4 m telescopes have a beam size (FWHM) of 2.′7 at the frequency of $C^{18}O$ ($J = 1$–0) line (109.782182 GHz). All the surveys have been done with a grid spacing of 2′, which corresponds to an actual resolution of 0.12 pc at a distance of 200 pc. It is small enough to resolve the dense cores of $n(H_2) \sim 10^4$ cm^{-3} embedded in the molecular clouds. The boundaries of the cores are uniformly defined as the half level of the peak intensity. The typical rms noise temperature for the survey in each region ranges from 0.15 K (Lupus and Southern Coalsack) to 0.25 K (Ophiuchus). The peaks of the cores are searched for down to 6σ detection which corresponds to the peak column density of $(4.5$–$7.5)\times10^{21}$ cm^{-2} in each region. The mass detection limits of the cores range from 0.7 $M_\odot$ to 1.3 $M_\odot$. Above this latter limit, the cores are uniformly surveyed and can be investigated statistically. The physical parameters of the cores are derived in the same manner for all the samples. The physical parameters of mass [$M/M_\odot$], average column density of H_2 [$N(H_2)$/cm^{-2}], radius [R/pc], line width [ΔV/km s^{-1}], number density of H_2 [$n(H_2)$/cm^{-3}], and virial mass [$M_{Vir}/M_\odot$] are estimated for each core. We assume the cores have uniform density, spherical shape, no contribution of external pressure, no support of magnetic fields, and no rotation for the calculation of M_{Vir}.

3. Results

3.1. Classification of the cores

In order to understand the relations between the core properties and the star-formation activity, we investigate the association of the YSOs with the cores. The YSOs are picked up by referring to the catalogues of IRAS point sources and T Tauri stars published elsewhere. From the distribution of the YSOs, significant concentrations can be seen as "clusters" with some specific cores such as the ρ Oph cloud. In such regions, stellar density of the YSOs is greater than 150 pc^{-3} (>10 stars within a typical radius of 0.25 pc), which corresponds to that of typical young star clusters (e.g., Lada & Lada 1991). In the whole Taurus cloud complex, about ∼100 YSOs are distributed in a volume of ∼500 pc^3, which yields the stellar density of only ∼0.2 pc^{-3}, much lower than above. On the other hand, many cores have no associated YSO, and are regarded as "starless" cores. The most interesting issue in this paper is where these varieties in the core activity come from.

In order to characterize the cores in terms of the star-formation activity, we classify the 179 cores into 3 categories according to the number of associated YSOs. We regard the YSOs which are located inside or within 2′ from the boundary of the cores as "associated" objects. The cores are then classified into starless, star-forming, and cluster-forming cores whose number of associated YSOs are 0, less than 10, and 10 or more, respectively. With these criteria, the number of cores is divided into 136, 36, and 7 for the categories respectively. Among the 7 cluster-forming cores, one is located in the CrA cloud, one in Lupus 3, two in the ρ Oph cloud, and three in the Cha I cloud.

Note that due to our definition of the cores, many of the apparent cluster members are not counted as associated objects, because the half-maximum intensity contours clip only the most intense parts of the $C^{18}O$ emitting area for very dense cores. There are many YSOs located outside of the outer bounds of such cluster-forming cores. In addition, the YSO surveys have been made deeply enough only in limited SFRs and it is difficult to know the total number of the YSOs in the entire system including fainter objects. Nonetheless, the high stellar density of relatively bright YSOs and the existence of a few massive stars such as the Herbig Ae/Be stars support that the total number of YSOs in the clusters is more than 100. In fact the ρ Oph cloud is reported to have more than 200 YSOs (Bontemps et al. 2001), and the Cha I cloud has ≥170 YSOs (Cambrésy 1998). Adams & Myers (2001) suggest that the stellar clusters with at least 100 members can survive to be observed as open clusters. The clusters in our definition coincide with their bona fide clusters and are supposed to become the open clusters.

In the following, we discuss the physical properties of the cores in terms of the star-formation activity as classified here.

Table 2. Average values of the physical parameters of the cores.

	starless		star-forming		cluster-forming
number of the cores	136		36		7
$N(H_2)(\times 10^{21}$ cm$^{-2})$	5.2	$<$	8.3	$<$	28.6
$n(H_2)(\times 10^3$ cm$^{-3})$	6.8	$<$	8.6	$<$	25.0
$M(M_\odot)$	15	$<$	32	$<$	155
R (pc)	0.19	$<$	0.23	$\lesssim$	0.25
ΔV (km s^{-1})	0.76	$\gtrsim$	0.72	$<$	1.31

3.2. Statistics of the physical parameters

The fundamental physical parameters of the cores, $N(H_2), n(H_2), M, R$, and ΔV, are derived and shown as histograms (Figs. 1). Starless, star-forming, and cluster-forming cores are designated by open, hatched, and shaded regions, respectively. Average values of the parameters for the 3 categories are also shown in Table 2.

For the parameters of $N(H_2)$, $n(H_2)$, and M, a significant trend can be seen in that star formation becomes more active as they increase, i.e., the cluster-forming cores have the largest values, the star-forming cores the middle, and the starless cores the smallest. This implies that when the cores get denser and more massive, star formation generally turns out to be active. This trend is most apparent for $N(H_2)$. There seems to be a threshold value for star formation, namely, more than 50% of the cores with $N(H_2) > 9 \times 10^{21}$ cm^{-2} show star or cluster formation. On the other hand, no clear trend can be seen for R and ΔV. Although the cluster-forming cores have again the largest values for them, the difference in R between the star-forming and the cluster-forming cores is small. The starless cores have even slightly smaller ΔV than the star-forming cores. This difference in ΔV will be discussed more in detail later in Sect. 4.4.

Our previous studies investigated these relations between the physical parameters and the star-formation activities in each region. This summarized work confirms that they are general trends commonly seen in the larger samples. Physical conditions that relate to star formation are probably uniform at least in the nearby regions.

3.3. Correlation analysis

In this section, we investigate some correlations among the physical parameters of the cores. There is a well-known empirical relation between R and ΔV (e.g., Larson 1981) and that is also reported for dense cores (Fuller & Myers 1992). The relation of the present sample is shown in Fig. 2. We see, however, no correlation among them. As will be mentioned in the later section, some of the cores are supposed to be disturbed by YSOs, nonetheless, even the starless $C^{18}O$ cores do not show any clear correlation. With this uniformly sampled core observed in a single tracer, the R and ΔV are scattered too much or both of their dynamic ranges are too small to firmly

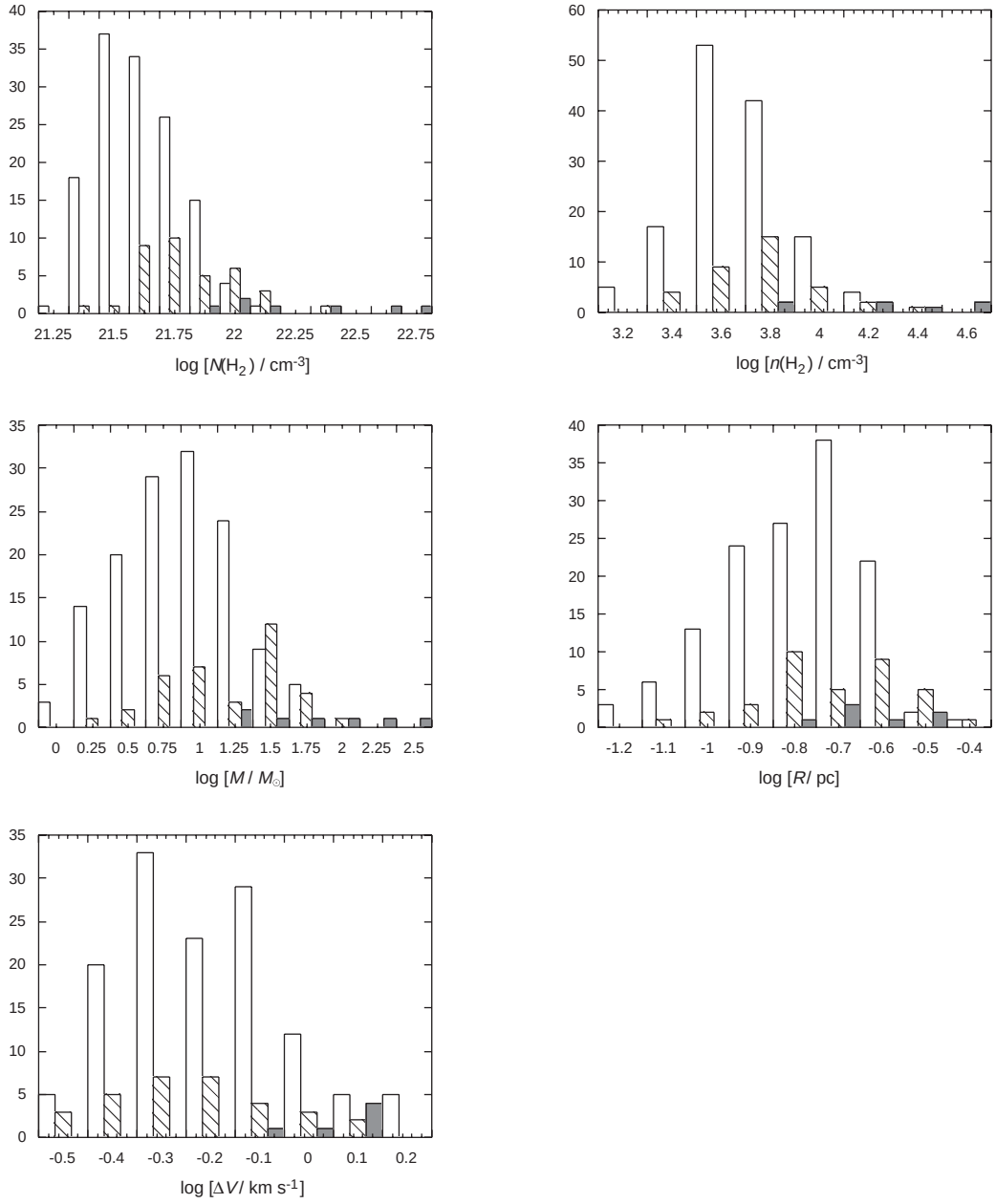

Fig. 1. Histograms of the physical parameters of the cores. Open, hatched, and shaded regions represent starless, star-forming, and cluster-forming cores, respectively.

establish dependence. As investigated in Ophiuchus (Tachihara et al. 2000), it is difficult to conclude the existence of the relation with the $C^{18}O$ cores, while the combined samples with ^{13}CO data taken in the same region show weak correlation with the help of relatively larger dynamic ranges. We see, however, no clear correlation with the larger number of the cores sampled uniformly. As summarized by Yonekura et al. (1997), unbiased surveys in optically thin single lines for smaller clouds than 2 pc tend to result in no or weak correlations between R and ΔV. In addition to this, studies for GMCs done in ^{12}CO seem to suffer from saturation of the optically thick line which makes the accurate estimations of ΔV difficult. As discussed by Lada et al. (1991), this relation strongly depends on the core definition. If multi-line surveys or different spatial resolution samples are included, they contaminate the correlation with different definitions. As will be mentioned in Sect. 4.2, ΔV of the $C^{18}O$ cores is dominated by the non-thermal turbulent gas motion. If the turbulence decays as the cores condense, and it has no internal and external input, it decreases monotonically. As low-density gas tracers tend to have larger ΔV, the R–ΔV relation may represent the *density–turbulence* relation (see also Sect. 4.1). However, the $C^{18}O$ molecular line traces the region with small density range and the large dispersion of ΔV is likely to come from the variety of the initial condition of the turbulence in the SFR. This probably makes the R–ΔV relation unclear in our sample.

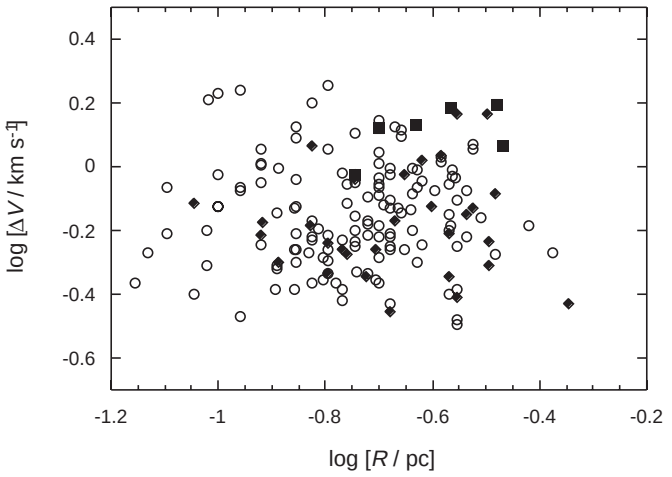

Fig. 2. Log-log plot of ΔV versus R. Open circles, diamonds, and squares denote the starless, star-forming, and cluster-forming cores, respectively.

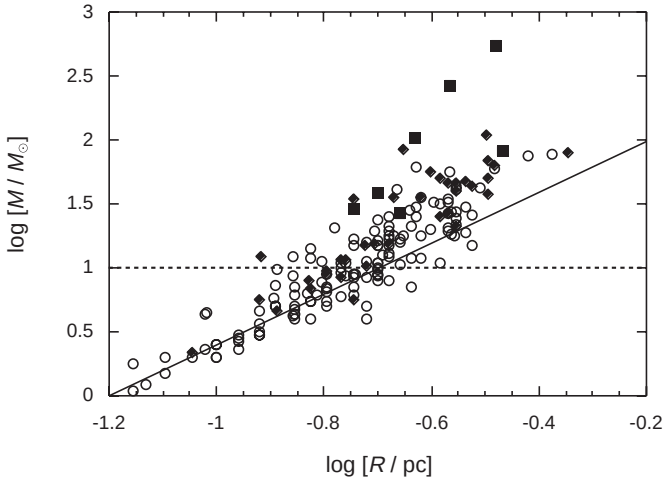

Fig. 3. Log-log plot of M versus R. Marks are the same as in Fig. 2. The dotted line shows $M = 10\ M_\odot$. The solid line denotes the relation of $M \propto R^2$.

We found positive correlations among R, M, and $N(\mathrm{H_2})$ as shown in Figs. 3 and 4. The core mass M increases basically as a function of R, there seem to be, however, two different trends. If M is smaller than $\sim$10 $M_\odot$, it follows nearly R^2 as shown by the solid line in Fig. 3, which means that M changes proportional to the projected area of the core extent keeping $N(\mathrm{H_2})$ as constant. When R and M becomes larger than 0.25 pc and 10 $M_\odot$, respectively, M and $N(\mathrm{H_2})$ increase significantly, keeping R constant. The same trend appears in Fig. 4. Low-mass cores have nearly constant $N(\mathrm{H_2})$ of $\sim 4\times10^{21}$ cm^{-2}, and massive cores roughly follow the best-fit function of $N(\mathrm{H_2}) \propto M^{0.74}$. The lower bound of $N(\mathrm{H_2})$ obviously comes from the detection limit due to the sensitivity. There is, however, no core with large R and small M (i.e. diffusely spread cores with low $N(\mathrm{H_2})$). These trends are reported by Onishi et al. (1996) and Tachihara et al. (2000), and confirmed with this larger number of cores.

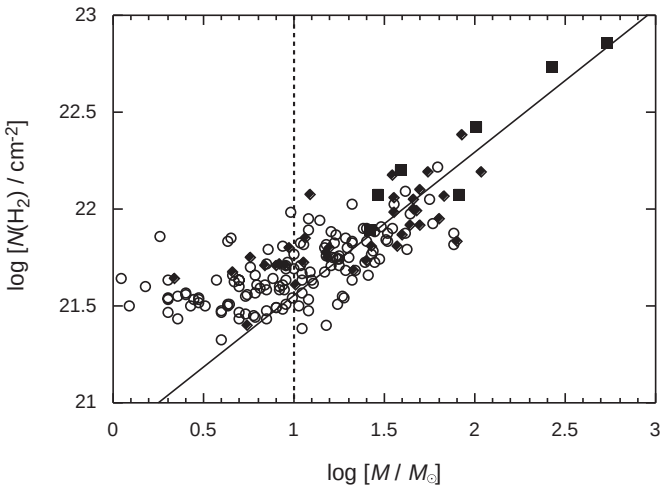

Fig. 4. Same as Fig. 3, but for $N_{\mathrm{H_2}}$ versus M. The solid line denotes the best-fit function of $N(\mathrm{H_2}) \propto M^{-0.74}$ for the cores of $M > 10\ M_\odot$.

3.4. Mass spectrum and the star-formation efficiency of the cores

As shown in Fig. 1, the distribution of the core mass roughly follows the lognormal distribution. We obtain the best-fit parameters of the mean value of $\log M = 1.09 \pm 0.02$ and $\sigma = 0.48 \pm 0.02$. This mean mass consistent with the Jeans mass with $n(\mathrm{H_2}) = 10^3$ cm^{-3} and $T = 20$ K, which are the typical density and temperature of the molecular clouds forming the dense cores.

It is worthwhile to compare the core mass spectrum to that of stellar initial mass function (IMF). In order to do that, the mass spectrum of the $C^{18}O$ cores are drawn in the conventional way, namely, the number of the cores per logarithmic mass bin is expressed as a power-law function of the core mass as $\mathrm{d}N/\mathrm{d}\log M \propto M^{-\Gamma}$ (Fig. 5). It shows that the mass spectrum is hardly fitted to a single power-law function. This trend was not clear for the previous studies in Taurus and Lupus, but slightly seen in Ophiuchus, maybe due to the limited number of samples and the smaller mass ranges in each region. Although it is not clear that the mass spectrum can be expressed as multiple power-law functions, we see slight turnovers around $M \sim 10\ M_\odot$ and $\sim$50 $M_\odot$. Thus we attempt to divide them into 3 mass ranges as $0.25 \leq \log M < 1$, $1 \leq \log M < 1.75$, and $1.75 \leq \log M$, and fit to 3 power-law functions. The calculated indices, Γ, for the 3 mass ranges are 0.25, 1.5, and 2.6, respectively. This result indicates that Γ is subject to change according to M. This may suggest that the fragmentation is not uniform throughout the cores with any mass and density. It is an interesting coincidence that we also see the turnover in Figs. 3 and 4 around $M \sim 10\ M_\odot$.

Note that most of the cores are supposed to fragment into smaller condensations through the contractions, thus the core mass function does not directory relate to the stellar IMF, unlike the smaller scale clumps detected in 1.3 mm dust continuum (Motte et al. 1998). Nonetheless,

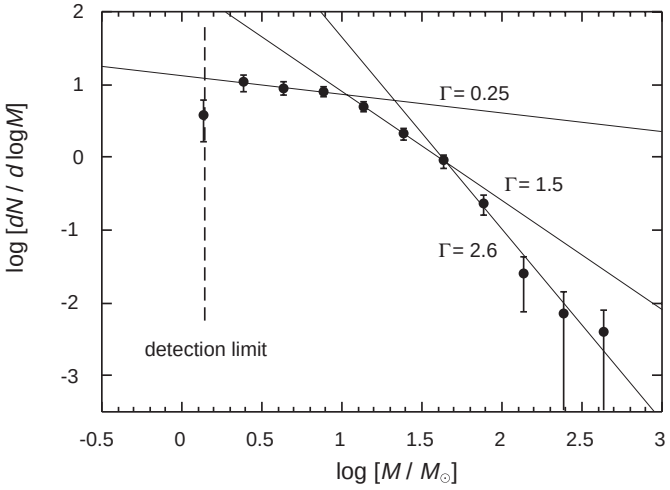

Fig. 5. Mass spectrum of the $C^{18}O$ cores. Three solid lines show the best-fit functions of different mass ranges (see text).

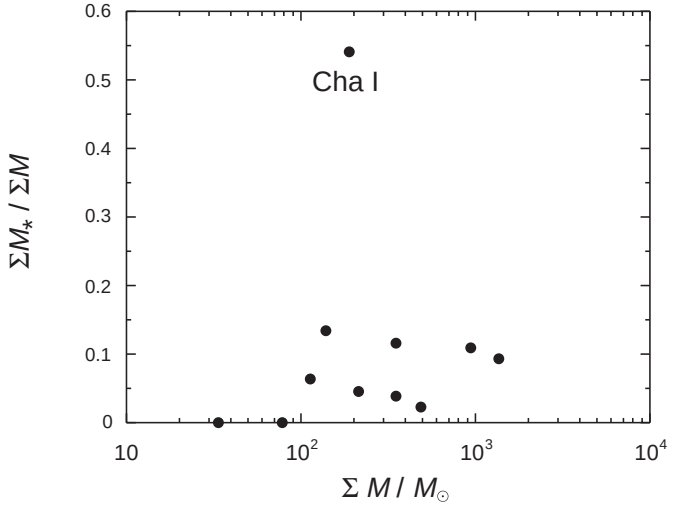

Fig. 6. Correlation between the total stellar mass divided by the total core mass and the total core mass for each SFR.

the similar trend can be seen for the stellar IMF. As is studied by many authors, the slope of the IMF is not uniform throughout the stellar mass range (e.g., Scalo 1986). It is nearly flat with $\Gamma \simeq 0.2$ for the very low-mass part ($M < 1\ M_\odot$), and steep with $\Gamma \simeq 1.7$ for $1\ M_\odot < M < 10\ M_\odot$.

A theoretical model is suggested by Nakano et al. (1995) that the cores have nearly constant star-formation efficiency (SFE; the ratio of the total mass of the formed stars to the core mass) almost independent of their mass and density, and is ∼4% for a uniform density gas sphere and ∼10% for critical iso-thermal sphere. Onishi et al. (1998) found that the SFE of the $C^{18}O$ cores in Taurus is a nearly uniform ∼10%. In order to confirm this general trend, we investigated the total mas ratio of the formed YSOs to the $C^{18}O$ cores, $\Sigma M_*/\Sigma M$, in each SFR (Fig. 6). Except for the Cha I cloud, this ratio ranges from 0% (the Cha III and the Southern Coalsack clouds) to 14% (the Cr A cloud) with the average value of 11% independently of ΣM. Note that the situations for some SFRs with the cluster-forming cores are different from that of Taurus, i.e., the SFEs of the cores are not uniform but different significantly from 20% (the ρ Oph cloud) or 40% (the CrA cloud) to 0% of many starless cores located in the same SFRs. Nevertheless, if we take the total mass of the cores and the YSOs throughout the SFR, they show about the same SFE of ∼10%. This trend is identical to the correlation between SFE derived from the ^{13}CO cloud mass ($M_{\rm cloud}$) and the core-to-cloud mass ratio ($\Sigma M/M_{\rm cloud}$) reported by Mizuno et al. (1999) and Tachihara et al. (2000).

If we apply SFE = 10% to the core mass spectrum, the expected stellar mass function agrees well with the stellar IMF, i.e., $\Gamma \simeq 0.25$ for $M_* < 1\ M_\odot$ and $\Gamma \simeq 1.5$ for $1\ M_\odot < M_* < 6\ M_\odot$. For the larger mass range of $M_* > 6\ M_\odot$, the Γ is steeper than that of the IMF although we have few samples in this range.

3.5. Dynamics of the cores

We investigate the dynamical stabilities for the cores employing virial analysis. The virial mass ($M_{\rm Vir}$) of the cores is estimated, excluding those with apparent multiple velocity components, from the radius and the line width as $M_{\rm Vir} = 210 R \Delta V^2$ by assuming that the cores have spherical shapes, uniform density, no external pressure, no magnetic support, and no rotation. If $M_{\rm Vir} > M$, the core cannot be gravitationally bound without external support, and do not collapse by overcoming the internal pressure spontaneously. We plot the $M_{\rm Vir}$ against the core mass (M) in Fig. 7, and the histogram of the virial ratio defined as $M_{\rm Vir}/M$ is shown in Fig. 8.

Many of the cores are distributed along the line which denotes the dynamical equilibrium ($M_{\rm Vir} = M$) and those cores that are nearly gravitationally bound, and 78% of them have a virial ratio of nearly unity ($|\log(M_{\rm Vir}/M)| < 0.5$). Smaller cores tend, however, to have larger $M_{\rm Vir}$ than M. Note that the ΔV is significantly larger than the typical thermal sound speed of $T \sim 10$ K. This means that the kinematics of the cores is dominated by the turbulent gas motion. Thus, the smaller cores generally have larger kinetic energy relative to the gravitational one.

There is also a significant difference in the virial ratio between the starless and the star-forming cores. More than 70% of the starless cores have $M_{\rm Vir} > M$, and seem to be gravitationally unbound. On the other hand, only 35% of the star-forming cores have $M_{\rm Vir} > M$ indicating that the star-forming cores are dynamically more relaxed. Their average virial ratios are 3.2 and 1.4, respectively. These clearly show that the gravitational energy dominates the star-forming cores even though some of the star-forming cores may be disturbed and their kinetic energies are enhanced by the formed YSOs. The star-forming cores do not necessarily have larger mass in the SFR such as L1333 and Oph North regions, while the

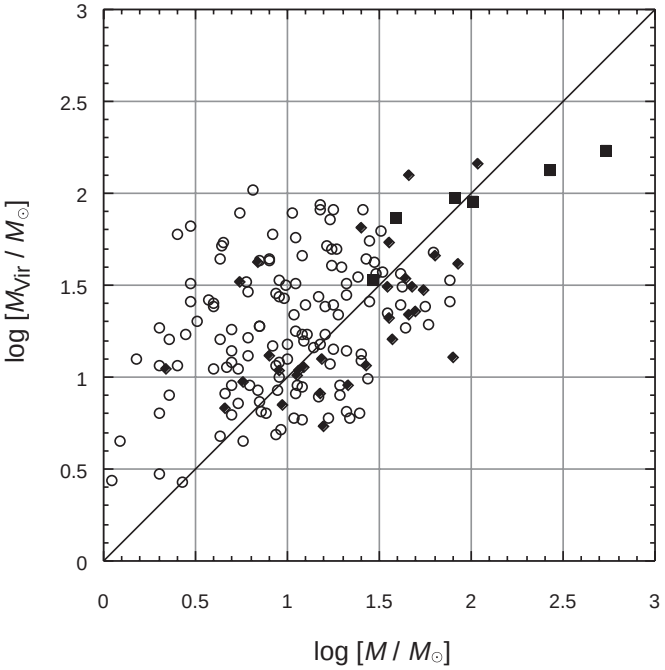

Fig. 7. Log-log plot of the virial mass, $M_{\rm Vir}$, against the core mass, M. The solid line represents the gravitational equilibrium. Marks are the same as in Fig. 2.

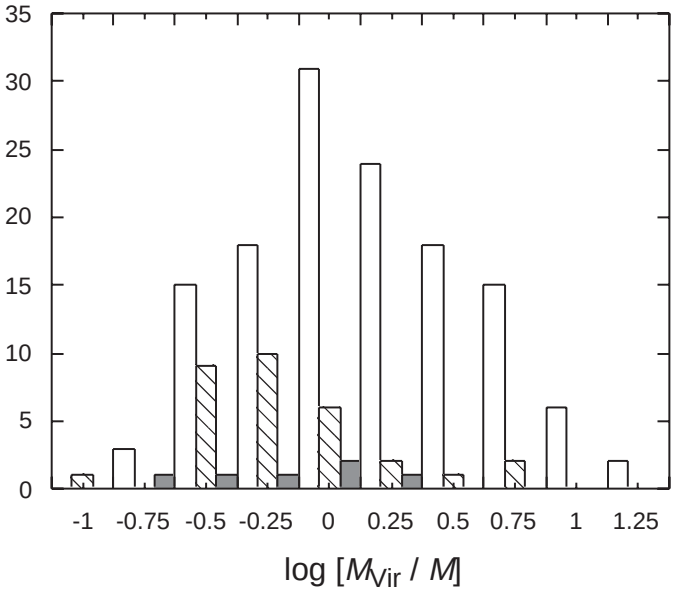

Fig. 8. Histogram of the virial ratio of the cores. Open, hatched, and shaded regions are the same as in Fig. 1.

trend between the virial ratio and star-formation activity is common for every SFR (Hara et al. 1999). This implies that the kinetic-energy loss by turbulent dissipation makes the virial ratio smaller, and this leads to star formation in the cores. This has been well discussed by Tachihara et al. (2000) and we confirm the trend with the present larger samples (more detailed discussion is given in Sect. 4.2). The virial ratio is, however, moderate for the cluster-forming cores. While the average virial ratio is 1.0, 50% of them have $M_{\rm Vir} > M$. This can be explained in that molecular outflow, stellar wind, and/or UV radiation of the formed YSOs may input kinetic energy into the cores, and make the virial ratios larger after the cluster-formation than those of star-forming cores. Some of them are expected to become dissipated in the near future.

4. Discussion

4.1. Comparison with the ammonia cores

There is a series of studies of NH_3 dense cores (e.g., Myers & Benson 1983), summarized by Jijina et al. (1999). The survey consists of 264 NH_3 cores in many SFRs, and some of the cores in the Taurus and Ophiuchus regions overlap with those in our $C^{18}O$ samples. It is quite interesting to make a comparison between these data. Among them, there are 35 nearby NH_3 cores catalogued in and around the Taurus and Ophiuchus regions. The NH_3 cores have a mean radius and density of 0.06 pc and 5×10^4 cm^{-3}, respectively, typically smaller and denser than the $C^{18}O$ cores by factors of $\sim$1/4 and $\sim$6, respectively (Myers et al. 1991). It seems that the emission lines of ammonia trace inner and denser parts of the cores. Actually in some of the $C^{18}O$ cores, multiple sub-clumps can be seen and NH_3 cores are detected at each peak. Denser gas condensations have been surveyed in the Taurus $C^{18}O$ cores with $H^{13}CO^+$ (J = 1–0) lines, which have a critical density of $n(H_2) \sim 10^5$ cm^{-3} (Mizuno et al. 1994; Onishi et al. 2001). The $H^{13}CO^+$ cores are detected near the peaks of the $C^{18}O$ cores or their sub-clumps as well. The difference between the NH_3 cores and the $H^{13}CO^+$ cores is still not clear; however, the NH_3 cores can be regarded as intermediate between the $C^{18}O$ and $H^{13}CO^+$ cores from their mean density and size although the spatial resolution of NH_3 is not sufficient. Apparently larger ΔV is detected for NH_3 cores with IRAS sources than those without (Fuller & Myers 1992; Myers & Fuller 1992; Jijina et al. 1999). This trend can also be seen for the $H^{13}CO^+$ cores (Mizuno et al. 1994) but not for the $C^{18}O$ cores. This is presumably because the YSOs formed with jets or outflows disturb the inner parts of the cores effectively (for more detail, see Sect. 4.4).

Generally speaking, the emission lines of ^{12}CO, ^{13}CO, $C^{18}O$, NH_3, and $H^{13}CO^+$ trace the different gas density regimes of $n(H_2) \sim 10^2$ cm^{-3}, 10^3 cm^{-3}, 10^4 cm^{-3}, 5×10^4 cm^{-3}, and $\geq 10^5$ cm^{-3}, respectively. Their typical line width changes as $\sim$2 km s^{-1}, $\sim$1 km s^{-1}, 0.76 km s^{-1}, 0.48 km s^{-1} (Jijina et al. 1999), and 0.48 km s^{-1} (Mizuno et al. 1994), respectively if the cores have no YSO. If one observes the denser parts, one generally obtains narrower lines. This presumably shows that the turbulence decays gradually leading to the gas condensation. Note that the turbulent motion still dominates the gas kinematics even with $n(H_2) \sim 10^5$ cm^{-3} overriding the thermal velocity dispersion. On the other hand, the cloud morphology is diffuse and/or filamentary if the density

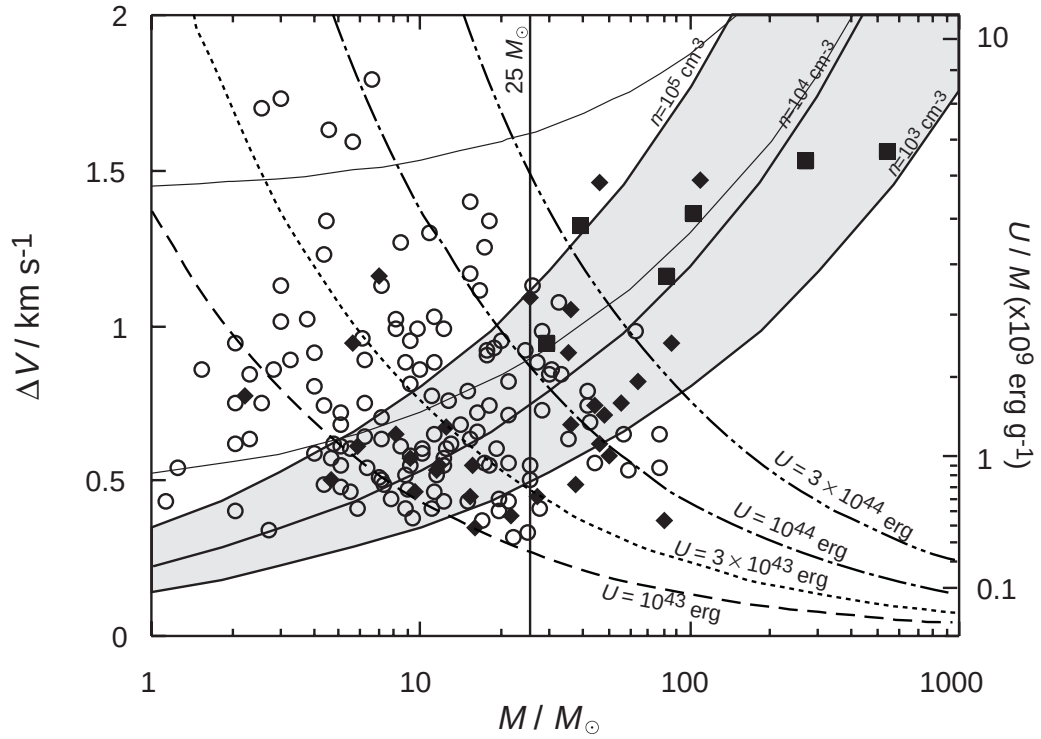

Fig. 9. Log-linear plot of ΔV versus M. Symbols are the same as in Fig. 2. Gray shaded area shows the region where the cores are in the virial equilibrium with $n(H_2)$ of between 10^3 cm^{-3} and 10^5 cm^{-3} when $P_{ext} = 0$. The two thin lines also denote the loci of the virial equilibrium with $n(H_2) = 10^4$ cm^{-3} for the cases of $P_{ext} = 1.7\times10^{-10}$ erg cm^{-3} (upper) and $P_{ext} = 1.7\times10^{-11}$ erg cm^{-3} (lower). Broken, dotted, dot-dashed, and two-dots-dashed lines show the loci of $U = 10^{43}, 3\times10^{43}, 10^{44}$, and 3×10^{44} ergs, respectively (see text).

is 10^{2-3} cm^{-3}. When the molecular gas gets denser than $n(H_2) \gtrsim 10^4$ cm^{-3}, its distribution becomes more spherical and can be called "cores". The average aspect ratios of $C^{18}O$ cores are 2.1 for Ophiuchus and 1.8 for Taurus, while that of NH_3 is 1.5. In addition to this, gas equilibrium changes from gravitationally unbound with $n(H_2) \lesssim 10^3$ cm^{-3} (Yonekura et al. 1997; Kawamura et al. 1998) to bound with $n(H_2) \gtrsim 10^4$ cm^{-3}. These facts imply that the self gravity dominates the gas dynamics against the turbulence when it gets denser, and the $C^{18}O$ cores with $n(H_2) \sim 10^4$ cm^{-3} are on the transient phase of the gas contraction between the turbulent dominant clouds and self-gravity dominant cores.

4.2. Star formation and turbulent gas motion in the cores

In order to investigate how the turbulent gas motion behaves as the cores evolve toward star formation, we compare ΔV between the starless and the star-forming cores as a function of M. Figure 9 is a log-linear plot of ΔV against M. If the cores are on the virial equilibrium with negligible external pressure, $M = M_{Vir} \equiv 210R\Delta V^2$ is achieved. If a uniform density is assumed as

$$n(H_2) = \frac{3M}{4\pi R^3 \mu m_H}, \quad (1)$$

where μ and m_H are the mean molecular weight and the atomic hydrogen mass, respectively; the virial equilibrium with constant $n(H_2)$ can be drawn by eliminating R from these formulae. Because the $C^{18}O$ emission line empirically traces the gas with smallest density range as 10^3 cm$^{-3} \lesssim n(H_2) \lesssim 10^5$ cm^{-3}, the cores in the virial equilibrium should be located within the gray region. In fact, the cores are surrounded by a considerable amount of molecular gas that produces the external pressure on the cores. By taking into account the external pressure, P_{ext}, the virial equilibrium can be written as

$$\frac{3M\Delta V^2}{8\ln 2} - \frac{3GM^2}{5R} - 4\pi R^3 P_{ext} = 0. \quad (2)$$

With the help of this effect, the gray region moves up following

$$\frac{\Delta V^2}{8\ln 2} = \frac{P_{ext}}{\rho} + \frac{G}{5}\left(\frac{4\pi\rho M^2}{3}\right)^{1/3}, \quad (3)$$

where and $\rho = \mu m_H n(H_2)$ as shown by the thin lines in Fig. 9 for the cases of $n(H_2) = 10^4$ cm^{-3} with $P_{ext} = 1.7\times10^{-11}$ erg cm^{-3} (typical case; Tachihara et al. 2000) and 1.7×10^{-10} erg cm^{-3} (10× typical case), and thus the cores above can be in virial equilibrium if the force balance is achieved.

In this figure, we see different trends between low-mass ($M < 25\ M_\odot$) and high-mass regions. This border of 25 $M_\odot$ roughly corresponds to the lower bound of

the cluster-forming cores. It can clearly be seen that ΔV is smaller for the star-forming cores than for the starless cores particularly in the low-mass region. For the low-mass cores, average ΔV of starless and star-forming cores are 0.77 $\mathrm{km\,s^{-1}}$ and 0.61 $\mathrm{km\,s^{-1}}$, respectively. It is also noticeable that these star-forming cores are nearly in the virial equilibrium or somewhat over-equilibrium as shown in Fig. 9 with the shaded area.

In order to evaluate this more quantitatively, the kinetic energies of the cores are investigated. The total kinetic energy, U, can be expressed as

$$U = \frac{3}{2}\frac{M\Delta V^2}{8\ln 2}\ [\mathrm{erg}] \quad (4)$$

and the 4 lines in Fig. 9 show the loci of constant U. The kinetic energy density per unit mass, U/M, which is just proportional to ΔV^2, is also shown as scales on the right side of Fig. 9.

For the low-mass cores, most of the star-forming cores have nearly constant U of $\sim 10^{43}$ ergs and only one of them has $U > 3 \times 10^{43}$ ergs, and only 3 star-forming cores have larger ΔV than 0.7 $\mathrm{km\,s^{-1}}$, which correspond to U/M of 1.3×10^9 erg $\mathrm{g^{-1}}$. On the other hand, U and ΔV of the starless cores range much wider. Seven low-mass starless cores have even larger U than 10^{44} ergs, and 5 have larger ΔV than 1.5 $\mathrm{km\,s^{-1}}$ corresponding to $U/M = 6 \times 10^9$ erg $\mathrm{g^{-1}}$. If the cores evolve from the starless to the star-forming cores keeping their masses as constant from up to down on the figure, the turbulent dissipation directly relates to the star-formation. It is suggested that such starless cores need to lose the kinetic energy of at least 10^{43-44} ergs to forming stars if M is constant through the contraction. When cores contract and get smaller, work done by the external pressure should be taken into account for the energy release additionally (see detail Tachihara et al. 2000). Because the differences in $n(\mathrm{H_2})$ and P_{ext} between the starless and the star-forming cores are expected to be small (see Fig. 1 and Table 2), this change of ΔV represents the turbulence dissipation and the dynamical relaxation, which lead to dynamical collapse and star formation.

It seems to be a more plausible view that cores get more massive by aggregating the envelope mass through evolution. If the cores get more massive keeping a uniform density and virial equilibrium, ΔV increases following the solid lines in Fig. 9. There are, however, a small number of starless and star-forming cores that have larger M and ΔV. This may mean that it is difficult to get more weight spontaneously without dissipating the turbulence through the evolution. The turbulent dissipation must be necessary also in this growing case. We naturally suggest that the spontaneous core evolution goes from left-top to right-bottom on the figure approaching the virial equilibrium by dissipating the kinetic energy.

Five of the 6 cluster-forming cores (excluding the apparently multi-peaked Lupus 3) have significantly greater U than 3×10^{44} ergs. This suggests that self-injection of the turbulence by the clusters is very effective. In the following subsections, non-spontaneous (namely triggered) cluster formation is discussed.

4.3. What makes cluster formations?

As shown in the previous sections, turbulent decay is a key issue for star formation. We could then ask, what makes cluster formation? The cluster-forming cores are only located in the ρ Oph, the CrA, Lupus 3, and the Cha I clouds. In order to understand the environments where the cluster-forming cores exist, we investigate the morphological structures of their parental ^{13}CO clouds shown in Fig. 10. It is noticeable that all of them show characteristic cloud structures, i.e., a massive head and long-spread tail, and the cluster formations are taking place at the heads of the clouds. The CrA cloud is one of the most prominent cases. The cloud has a cometary shape pointing toward the Sco OB 2 association and the Cornet cluster is located in the massive core at the top of the cloud (Wilking et al. 1997). The ρ Oph cloud also has a massive head where active cluster formation occurs, and a few long filamentary tails (Loren 1989). Although there are 3 cluster-forming cores in the Cha I cloud, the most active cluster formation can be seen at the northern top of the ridge (Mizuno et al. 1999). These facts suggest that the clouds have been affected by external shocks, and the shocks have triggered active cluster formation. Actually, a shock triggering scenario is suggested for ρ Oph cloud by many authors (Vrba 1977; Loren & Wootten 1986; de Geus 1992; Preibisch & Zinnecker 1999). An expanding HI shell centered Upper-Scorpius subgroup of the Sco OB 2 shows the shock hitting the cloud, and this may be also the case for Lupus 3 (Tachihara et al. 1996, 2001). It is not so clear for the Cha I cloud; however, Mizuno et al. (2001) recently suggest from the existence of an HI expanding shell that such a shock may affect the Chamaeleon clouds as well. Thus, external shock effects such as supernova explosion and stellar wind from OB stars are likely to form the head-tail structure of the clouds and trigger the cluster-formation in the head.

4.4. Initial conditions and enhancement of the turbulence

As mentioned in Sects. 3.5 and 4.2, the kinetic support of the cores by turbulence plays an important role for the core evolution and star formation. Then we expect that the time scale of the star formation may be determined by the initial amount of the turbulent energy and its dissipation and input rates. It is, therefore, interesting to investigate the difference in initial conditions of the turbulence among the SFRs. If one accepts the hypothesis that the turbulence is provided only by the formed stars and dissipates monotony without YSOs, one can estimate the initial amount of the turbulence from the ensembles of only the starless cores. We compare the average ΔV for

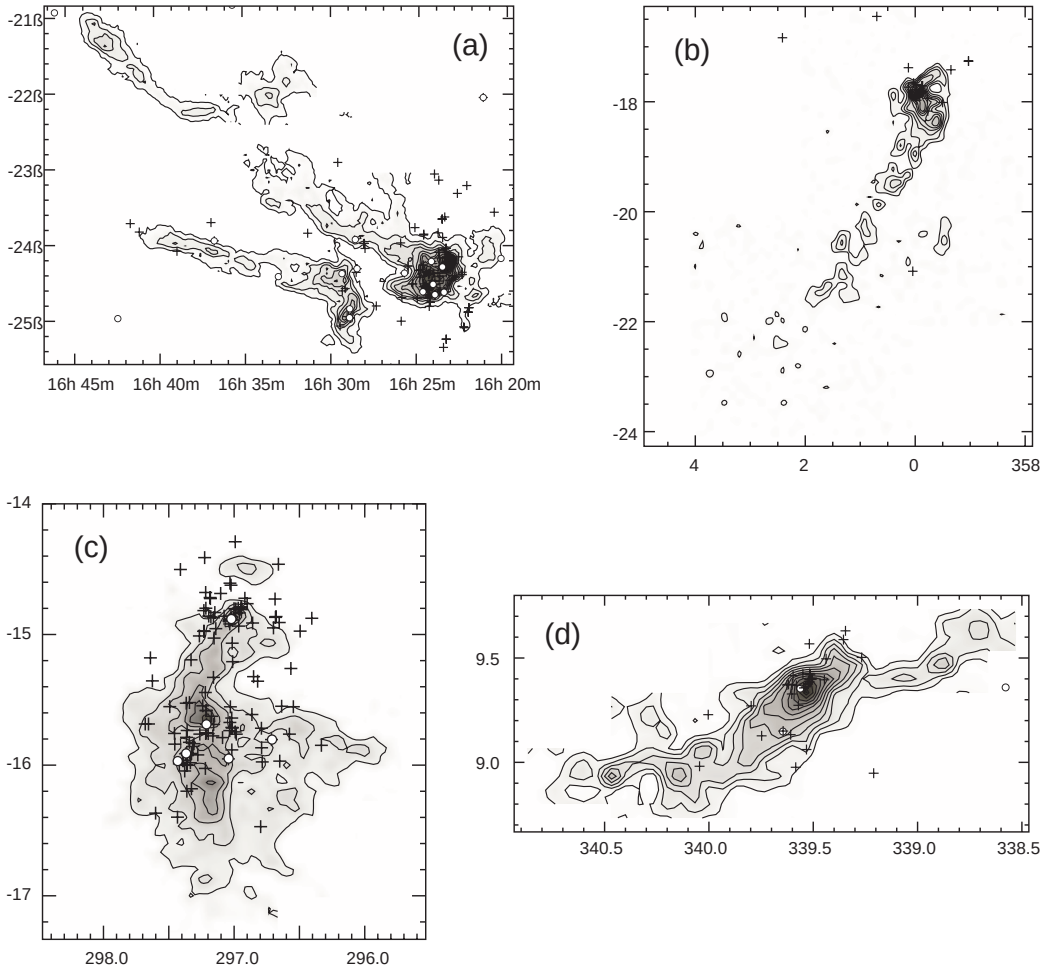

Fig. 10. Gallery of the ^{13}CO clouds that contain cluster-forming cores inside. The integrated intensity maps of **a)** the ρ Oph, **b)** the CrA, **c)** the Cha I, and **d)** the Lupus 3 clouds are drawn in contours and gray scale. Crosses and circles are associated pre-main sequence stars and protostellar IRAS point sources, respectively.

the starless cores which have not been disturbed by YSOs and may still reflect the initial conditions.

Figure 11 shows SFEs estimated from the total mass of ^{13}CO clouds ($M_*/[M_* + M_{\rm cloud}]$) plotted against ΔV averaged over only the starless cores in each SFR. Note that the SFE changes so much depending on its definition. Very high SFEs have been estimated for the most active "head" parts to be ∼40% for the CrA cloud (Harju et al. 1993) and ∼22% for the ρ Oph cloud (Wilking et al. 1989) based on $C^{18}O$ mass. In order to investigate the general star-forming activity of the whole SFR, the SFEs should be revised based on the ^{13}CO mass. Recent mid-IR survey with ISO satellite revealed a large number of newly identified YSOs in the ρ Oph cloud (Bontemps et al. 2001). The total mass of the young star cluster is estimated to be 102 $M_\odot$. There are about 50 more YSO candidates of Hα emission-line stars (Wilking et al. 1987) and IRAS point sources in the peripheral and the filamentary-cloud regions, even though the YSO survey is insufficient there. If we take into account the mass of these stars (assuming a typical mass of 0.5 $M_\odot$), the entire SFE of the ρ Oph cloud derived from the ^{13}CO mass of 3050 $M_\odot$ (Loren 1989) is calculated to be ∼4%. For the CrA cloud, the total ^{13}CO cloud mass has not been given yet. If we apply the ratio of the total $C^{18}O$ core mass to the ^{13}CO cloud mass to be 30% (same as the ρ Oph cloud; Mizuno et al. 1999), the SFE is diluted to ∼4%. Many of these values are lower limits because of the incomplete YSO survey.

We find that all the active SFRs whose ^{13}CO-based SFE is greater than 2% (the CrA, ρ Oph, Cha I, and Taurus clouds) have $\Delta V < 0.7$ km s^{-1}. On the other hand, all the other less active SFRs have $\Delta V > 0.7$ km s^{-1} except for the Pipe nebula. The SFRs which contain the cluster-forming cores (filled squares) have smaller ΔV except for Lupus, while the SFR without them (open circles) have larger ΔV except for Taurus. We expect that the initial amount of turbulence in a SFR determines the SFE as a whole.

As mentioned in the last section, cluster-forming cores are located in the head parts of the elongated clouds, and the starless cores are in generally the long-spread filaments. The cluster-forming cores are significantly more massive than the others, and the external shocks seem to aggregate the mass on the head parts of the clouds

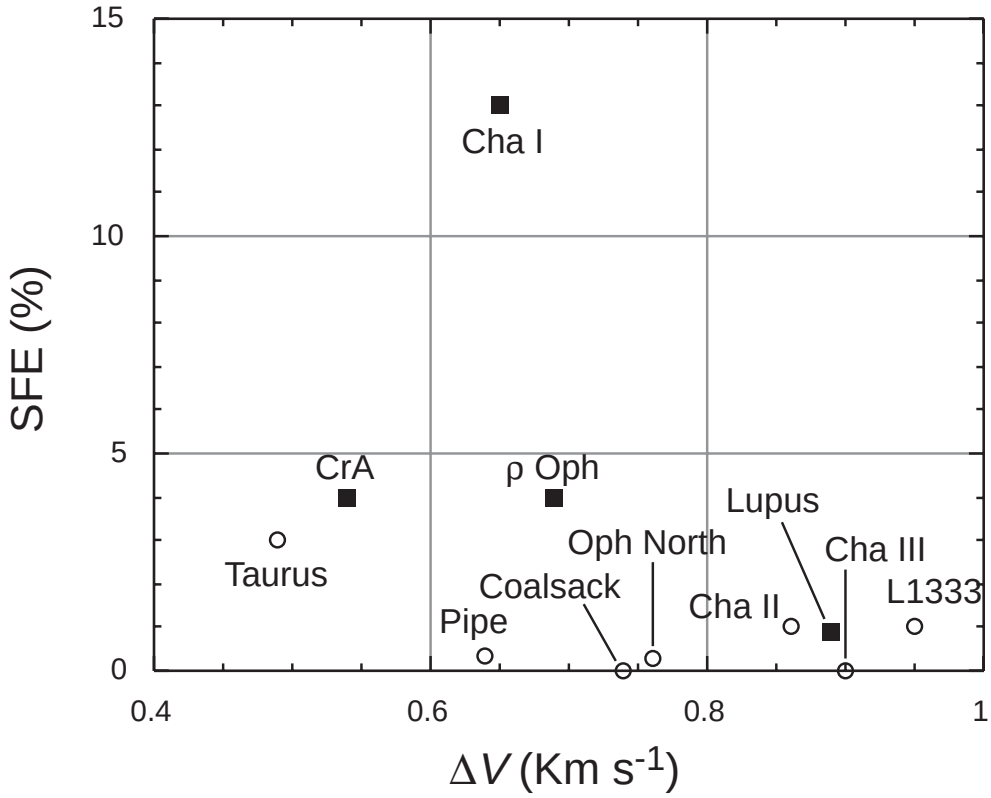

Fig. 11. Correlation diagram of SFE against ΔV averaged over only the starless cores for each SFR. Squares and circles denote the region with and without cluster-forming cores, respectively.

effectively. On the other hand, although these filaments are also supposed to be formed under the influence of the shock wave, the cores in them do not show any enhancement of ΔV. Note that we regard Lupus clouds as one SFR here although it contains several individual molecular clouds (Hara et al. 1999), and Lupus 3 is the only active and cluster-forming cloud among them.

From these facts, we suggest the following idea. If a SFR has initially more turbulent energy in the molecular gas, it takes longer to dissipate the energy so that it is small enough to form stars, resulting in low SFE. If the initial turbulent energy is small, a molecular cloud forms stars spontaneously and shows moderately large SFE, like Taurus. When a shock wave affects a molecular cloud which has smaller turbulence, it makes a head-tail structure in the cloud and triggers cluster formation in the head. The shock wave, however, does not enhance the turbulence effectively.

Next we investigate the turbulent input from the YSOs to the cores. It seems to be very difficult to estimate how much kinetic energy can be fed back by the young stars because of the uncertainty in the physical parameters. Let us, however, roughly estimate how much energy a molecular outflow from a young star can produce. By assuming the mass-outflow rate as $\dot{M} = 10^{-6}\ M_\odot\ \mathrm{yr}^{-1}$, outflow velocity as $v = 10\ \mathrm{km\,s}^{-1}$, the time scale of the outflow as $\tau = 10^5$ yr (Fukui 1989, 1993), and energy conversion coefficient as $\epsilon = 1\%$, then the energy input of $\frac{1}{2}\epsilon\tau\dot{M}v^2 \sim 10^{42}$ ergs can be achieved by a single star. If the quantities of some of the parameters are smaller than assumed above, the star-forming cores still have relatively lower kinetic energy. With a hundred of YSOs, it is plausible to enhance the turbulence by more than 10^{44} ergs. For the smaller and denser cores detected in NH_3 and $H^{13}CO^+$, it is easier to disturb the cores entirely by the outflow from only a single star, because the kinetic energy of these smaller cores are estimated to be one order of magnitude smaller than that of the $C^{18}O$ cores. Other physical processes of turbulent enhancement such as stellar wind and UV radiation from the YSOs should also be taken into account. Thus, significantly greater turbulence in the cluster-forming cores can be explained by the disturbance of the young stellar clusters.

5. Summary

From the large systematic survey of the dense molecular cloud cores taken with the NANTEN and the 4 m radio telescopes, we made a statistical study of the core properties from the view of the star and cluster formation. The main results are follows.

1. Nine nearby star-forming regions are surveyed for dense cores in $C^{18}O$ and 179 cores are collected.
2. The cores are classified into 3 categories in terms of their star-formation activities as starless, star-forming, and cluster-forming cores. The numbers of cores in each category are 136, 36, 7, respectively.

3. Physical parameters of the cores are estimated. Cores with active star formation tend to have larger M, $N(H_2)$, and $n(H_2)$. Particularly, there seems to be a threshold value of $N(H_2)$ at $\sim 9 \times 10^{21}$ cm^{-2}.
4. Virial analysis of the cores shows that most of the cores are gravitationally bound and that the virial ratios are close to the unity. The star-forming cores have significantly smaller virial ratios than others. This means that they are gravitationally more relaxed and turbulent dissipation is needed to form stars. Some of the cluster-forming cores are unbound and should be dissipated near future.
5. The SFE derived from the total mass of the $C^{18}O$ cores in the whole SFR is a nearly constant $\sim$10%, independent of the total core mass.
6. The mass spectrum of the cores is poorly fitted by a single power-law function. The power-law index is subject to change from 0.25 in the low-mass range to 2.6 in the high-mass range. If the 10% efficiency is applied to the mass spectrum of the cores, the expected stellar mass function approximates the stellar IMF.
7. Particularly for the low-mass cores, we found that star-forming cores have a smaller ΔV than the starless cores of the same mass range. This indicates the turbulent decay leads to star formation in the cores.
8. The molecular clouds with cluster formation all have head-tail structures, and the cluster-forming cores are located in the heads. The external shock interaction is suggested to form the cloud structures and trigger cluster formation.
9. In order to investigate the initial conditions of the turbulence, the average ΔV of the starless cores in the SFRs are investigated. The results suggest that the active SFRs have smaller ΔV and may have initially smaller turbulent energies. The shock wave that triggers cluster formation does not seem to enhance the ΔV effectively, while the formed clusters can do so by injection of kinetic energy of $\sim 10^{44}$ ergs.

Acknowledgements. We are grateful to all the staff of the Las Campanas Observatory for the great hospitality. The data for Chamaeleon, Southern Coalsack, Lupus, Pipe nebula, and the CrA cloud regions were taken during the NANTEN project based on mutual agreements between Nagoya University and the Carnegie Institution of Washington. This project was realized with the contributions from many Japanese public donors and companies. This work was financially supported in part by Grants-in-Aid for Science Research from the Ministry of Education, Science, Sports, and Culture (No. 10147208). Two of the authors (AM and YF) acknowledge financial support from the scientist exchange program under a bilateral agreement between JSPS (Japanese Society for the Promotion of Science) and CONICYT (the Chilean National Commission for Scientific and Technological Research).

References

Adams, F. C., & Myers, P. C. 2001, ApJ, 553, 744
Bontemps, S., André, P., Kaas, A. A., et al. 2001, A&A, 372, 173
Cambrésy, L., Copet, E., Epchtein, N., et al. 1998, A&A, 338, 977
de Geus, E. J. 1992, A&A, 262, 258
Fukui, Y. 1989, in Low Mass Star Formation and Pre-main Sequence Objects, ed. B. Reipurth (Garching: ESO), 95
Fukui, Y. 1993, in Protostars and Planets III, ed. E. H. Levy, & J. I. Lunine (Tucson: The University of Arizona Press), 603
Fuller, G. A., & Myers, P. C. 1992, ApJ, 384, 523
Hara, A., Tachihara, K., Mizuno, A., et al. 1999, PASJ, 51, 895
Harju, J., Haikala, L. K., Mattila, K., et al. 1993, A&A, 278, 569
Jijina, J., Myers, P. C., & Adams, F. C. 1999, ApJS, 125, 161
Kato, S., Mizuno, N., Asayama, S., et al. 1999, PASJ, 51, 883
Kawamura, A., Onishi, T., Yonekura, Y., et al. 1998, ApJS, 117, 387
Kenyon, S. J., & Hartman, L. W. 1995, ApJS, 101, 171
Lada, E. A., Bally, J., & Stark, A. A. 1991, ApJ, 368, 432
Lada, C. J., & Lada, E. A. 1991, in The Formation and Evolution of Star Clusters, ed. K. Janes (San Francisco: ASP), ASP Conf. Ser., 13, 3
Larson, R. B. 1981, MNRAS, 194, 809
Loren, R. B. 1989, ApJ, 338, 902
Loren, R. B., & Wootten, A. 1986, ApJ, 306, 142
Mizuno, A., Hayakawa, T., Tachihara, K., et al. 1999, PASJ, 51, 859
Mizuno, A., Onishi, T., Hayashi, M., et al. 1994, Nature, 368, 719
Mizuno, A., Yamaguchi, R., Tachihara, K., et al. 2001, PASJ, 53, 1071
Motte, F., Andre, P., & Neri, R. 1998, A&A, 336, 150
Myers, P. C., & Benson, P. J. 1983, ApJ, 266, 309
Myers, P. C., & Fuller, G. A. 1992, ApJ, 396, 631
Myers, P. C., Fuller, G. A., Goodman, A. A., & Benson, P. J. 1991, ApJ, 376, 561
Nakano, T., Hasegawa, T., & Norman, C. 1995, ApJ, 450, 183
Neuhäuser, R., Walter, F. M., Covino, E., et al. 2000, A&AS, 146, 323
Nozawa, S., Mizuno, A., Teshima, Y., Ogawa, H., & Fukui, Y. 1991, ApJS, 77, 647
Obayashi, A., Kun, M., Sato, F., Yonakura, Y., & Fukui, Y. 1998, AJ, 115, 274
Onishi, T., Kawamura, A., Abe, R., et al. 1999, PASJ, 51, 871
Onishi, T., Kawamura, A., Tachihara, K., Mizuno, A., & Fukui, Y. 2001, ApJ submitted
Onishi, T., Mizuno, A., Kawamura, A., Ogawa, H., & Fukui, Y. 1996, ApJ, 456, 815
Onishi, T., Mizuno, A., Kawamura, A., Ogawa, H., & Fukui, Y. 1998, ApJ, 502, 296
Preibisch, T., & Zinnecker, H. 1999, AJ, 117, 2381
Scalo, J. M. 1986, Fund. Cosmic Phys., 11, 1
Tachihara, K., Dobashi, K., Mizuno, A., Ogawa, H., & Fukui, Y. 1996, PASJ, 48, 489
Tachihara, K., Mizuno, A., & Fukui, Y. 2000, ApJ, 528, 817
Tachihara, K., Toyoda, S., Onishi, T., et al. 2001, PASJ, 53, 1081
Vrba, F. J. 1977, AJ, 82, 198
Wilking, B. A., Lada, C. J., & Young, E. T. 1989, ApJ, 340, 823
Wilking, B. A., McCaughrean, M. J., Burton, M. G., et al. 1997, AJ, 114, 2029
Wilking, B. A., Schwartz, R. D., & Blackwell, J. H. 1987, AJ, 94, 106
Yonekura, Y., Dobashi, K., Mizuno, A., Ogawa, H., & Fukui, Y. 1997, ApJS, 110, 21
Yonekura, Y., Mizuno, N., Saito, H., et al. 1999, PASJ, 51, 911